A method to estimate battery SOH indicators based on vehicle operating data only

Loïc Vichard, Alexandre Ravey, Pascal Venet, Fabien Harel, Serge Pelissier, Daniel Hissel

Version of Record: https://www.sciencedirect.com/science/article/pii/S0360544221004849
Manuscript_6fb262d58c426301b03cdaf979bfd50f

A method to estimate battery SOH indicators based on vehicle operating data only

L. Vichard[a,b], A. Ravey[a,b], P. Venet[b,c], F. Harel[b,d], S. Pelissier[b,d], D. Hissel[a,b]

[a] *FEMTO-ST Institute, CNRS, Univ. Bourgogne Franche-Comté, UTBM, Belfort, France*
[b] *FCLAB, CNRS, Belfort, France*
[c] *Univ Lyon, Université Claude Bernard Lyon 1, Ecole Centrale de Lyon, INSA Lyon, CNRS, Ampère, F-69622, Villeurbanne, France*
[d] *AME-Eco7, Univ Gustave Eiffel, IFSTTAR, Univ Lyon, F-69675 Lyon, France*

Abstract

Batteries are multi-physical systems and during actual operating conditions they are submitted to variable ambient operating conditions which can affect the dynamic behavior and the degradation. Therefore, a good understanding of the dynamic behavior and the degradation laws under actual operating conditions is the key to a durability improvement and to the development of better energy management strategies. The purpose of the proposed study is to use an experimental database issued from a three years monitoring of a ten postal vehicle fleet to model the batteries with respect to operating conditions. Based on an electrical circuit model, an optimization algorithm and a Kalman filter, the scientific contribution is to propose a simple but efficient method, using vehicle operating data only, to estimate on-board the state of charge and state of health indicators linked to internal resistance and available capacity. The proposed model presents a very good accuracy and state of health indicators estimations show promising results. In the future, the proposed method could be applied on-board to estimate and analyze the state of health during the entire battery lifetime in order to provide an accurate state of charge estimation and to contribute to a better understanding of the degradation laws.

Keywords— Battery SOH, Battery modeling, Vehicle operating data, Electric vehicle

1. Introduction

Nowadays, greenhouse gas emissions have to be significantly reduced. This is the reason why the popularity of low emission vehicles such as Electric Vehicles (EVs), Hybrid Electric Vehicles (HEVs) and Fuel Cell Hydrogen Electric Vehicles (FCHEVs) is highly growing [1–3]. Consequently, batteries used in transportation applications became a famous topic. However, batteries are frequently pointed out because of their high prices but also because of their low autonomy, low durability and their long time recharge which are limitations to a worldwide deployment [4].

Battery performances degrade with the repeatedly charging and discharging [5] and because of calendar aging [6, 7]. Batteries are multi-physical systems and operating conditions can affect the dynamic behavior and the degradation in different manners [8, 9]. Moreover, as the batteries degrade overtime depending on the operating conditions, the battery maximum discharge capacity decreases during the long-term operation and affects the accuracy of the State Of Charge estimation (SOC). Therefore, a good understanding of the dynamic behavior and the degradation mechanisms occurring during actual operating conditions is of particular importance to improve the durability with the development of better materials and energy management strategies. To tackle this issue, a first step is to master a good online degradation quantification of the battery component.

The battery State of Health (SOH) is commonly used as a metric to quantify the aging level of a battery [10, 11]. The SOH often refers to either the capacity fade [12, 13] or to the power fade [13]. The capacity fade refers to the loss in capacity (in Amps hours) of the component and the power fade refers to the internal impedance increment. On the one hand, accurate online estimation results are helpful to ensure the system running safely and to estimate precisely the SOC. On the other hand, SOH evolution can be analyzed with respect to operating conditions in order to contribute to a better understanding of the degradation laws.

A wide variety of studies have focused on SOH estimation [10, 11]. The proposed approaches can be classified according to three differents categories: (1) direct measurement approaches, (2) data driven approaches and (3) model-based approaches. Each category has its own advantages and drawbacks in terms of accuracy, computational requirement, testing time or cost.

(1) Direct measurement approaches: these methods use raw measured data to estimate SOH without reproducing the dynamic behavior of the battery. For example, from the perspective of determining the battery capacity, Kong et al. [14] proposed a coulomb counting method to estimate the SOC and the SOH of a battery cell. Coulomb counting methods are very basics and do not consider operating conditions [10]. Moreover, an accumulated error and sensor noise can lead to significant estimation errors.

Some other studies proposed Open Circuit Voltage (OCV) based methods to determine the battery capacity by using the relationship between the OCV and the SOC [15, 16]. OCV based methods can be performed in both online or offline states. Nonetheless, laboratory tests are necessary to determine the relationship between OCV and SOH.

Electrochemical Impedance Spectroscopy (EIS) has also been considered as a tool to estimate battery SOH [17–20]. Based on a Nyquist diagram, raw data can be used to identify easily a degradation. Another way to estimate SOH with EIS is to correlate Nyquist diagrams with the parameters of an Electrical Circuit Model (ECM). Although EIS provides very consistent information about the battery state and shows very good accuracy to

Nomenclature

BMS	Battery management system
DVA	Differential voltage analysis
ECM	Electrical circuit model
EIS	Electrochemical impedance spectroscopy
EKF	Extended Kalman filter
$FTP-75$	EPA Federal Test Procedure
ICA	Incremental capacity analysis
$LifePO_4$	Lithium iron phosphate
$NEDC$	New European Driving Cycle
OCV	Open circuit voltage
SOC	State of charge
SOF	State of function
SOH	State of health
$WLTP$	Worldwide harmonized Light vehicles Test Procedures

estimate ECM parameters, this tool is still more dedicated to laboratory applications as online applications are not yet well mastered. However, several studies have shown promising results and assure that EIS can be integrated in a vehicle by controlling the harmonic injection in the system to be characterized via the static converter [21, 22].

Incremental Capacity Analysis (ICA) and Differential Voltage Analysis (DVA) are both interesting methods that have been focused on. These methods provide information about the internal cell state using only the cell voltage and current measurements during a constant recharge or discharge [23–25]. ICA refers to the ratio between a quantity of electric charges and a voltage variation and DVA is the mathematical inverse. Some studies used these methods during battery charging to analyze the dynamic behavior and quantify the SOH [23–26]. Both methods are very promising and show very consistent results. However, as mentionned in Dubarry et al. [23], the consistency of the obtained information are directly linked to the current value: the lower the charging current the best the information, which can be very problematic in the case of vehicle applications.

(2) Data driven approaches: data driven methods have also been used to estimate battery SOH. This approach does not consider the physical laws of the battery system as the methods are purely based on data-driven tools such as artificial neural networks [27–29], support vector machine [30, 31] or again deep learning [32]. Although these black-box approaches can provide good estimation accuracy, they require a large amount of data for the training and high computational load. Because of these constraints, these methods may not be suitable for on-line real-time purpose as BMS often contain some microcontrollers or low computing performance systems.

(3) Model based approaches: a large number of studies have focused on the use of battery models to identify degradation and estimate the SOH [10, 33, 34]. Models are used to reproduce the dynamic behavior of a battery: voltage response as a function of inputs such as current, temperature and SOC. Model parameters have certain relationships with the battery aging level. Thus, they can be used to estimate the SOH and their evolutions can be investigated overtime and correlated with operating conditions to analyze degradation laws. It is worth remembering that operating conditions such as SOC, temperature, current etc. affect battery degradation and dynamic behavior. Thus, many parameters are interdependent and empirical models can tend to be complex. This is the reason why electrical circuit models (ECM) and electrochemical models are commonly used. Electrochemical models are generally exploited to understand electrochemical phenomena. This kind of model is more complicated to implement as it needs many physico-chemical parameters as inputs and lead to important computational requirements [35–37]. In contrast, ECM have been extensively studied in the literature for SOH estimation applications [38–42]. These approaches exhibit low complexity, low computational requirement and acceptable estimation accuracy. Ren et al. [41] proposed a method based on an ECM and a Kalman filter to estimate SOC and SOH indicators of a battery pack. The method has been tested with Hybrid Pulse Power Characterization (HPPC) profiles and showed promising accuracy. Shen et al. [39] proposed a method to estimate concurrently the SOC, the SOH, and the state of function (SOF) for lithium-ion batteries in real-time applications. The battery capacity was estimated according to the accumulated charge between two specific moments with online OCV identification. Based on the capacity update from SOH estimation, the SOC could be estimated according to the battery aging. The tests were performed with HPPC profiles. Although the presented results show good accuracy, this method is based on OCV curves. Therefore, the method can be hard to be applied on other technologies such as $LiFePO_4$ which presents a relatively flat OCV curve for SOC between 80% and 20%.

Given the previous cited studies, an ECM based method has been preferred in our study to estimate internal resistance and battery capacity as SOH indicators. It is worth noting that SOH estimation accuracy depends on the model accuracy. Consequently, the first step is to build an accurate and suitable model for real applications.

The large majority of SOH estimation methods published in the literature are based on laboratory tests or simplified driving cycles such as NEDC, FTP-75 or WLTP. Despite the greatest attention given to these studies, the generated electrical solicitations may not fully reflect the battery dynamic behavior operating in real applications. Therefore, the use of raw vehicle operating data directly issued from monitoring is essential to build more accurate models and more reliable SOH estimation methods.

In this framework, the main contribution of this study is to propose a simple and accurate model-based method to estimate both SOH indicators (capacity and internal resistance), of a $LifePO_4$ battery by using only physical values measured on-board during real driving cycles. In a first part the experimental context of the project and its application

will be introduced. In a second part, the method to build the battery cell model considering the operating condition and to identify online the internal resistance will be detailed. In a third part a method based on an extended Kalman filter to estimate concurrently the SOC and the battery capacity will be exposed. Finally conclusion and perspectives will be drawn.

2. Experimental context

2.1. Vehicle fleet

Mobypost was a european project which aimed at developing a fleet of ten experimental fuel cell hydrogen electric vehicles (cf. Figure 1) dedicated to postal delivery applications [43],[44]. The vehicles were designed considering the ability to support an important number of starts and stops and also the possibility to operate with the fuel cell off. The power-train integrated two power sources : a $LiFePO_4$ battery pack and a fuel cell system.

The battery pack is composed of four modules connected in series. Each module presents a nominal voltage of 12.8V at 23°C. Nominal capacity given by the manufacturer is 110Ah at 23°C with a discharge current of C/5. Each module integrates four cell groups connected in series which are composed of $LiFePO_4$ 3.2V cells connected in parallel to reach a capacity of 110Ah. The battery temperature values are measured inside each module.

A deep monitoring of the vehicles during the three years of experimentation led to create a rich database. More than one hundred physical variables from all the vehicle components were measured and saved on a server every second such as battery cell voltages, battery current, battery temperature, battery SOC, fuel cell system voltage and current, hydrogen tank SOC, vehicle speed, gps location to cite the main variables.

Figure 1: Three vehicles of the vehicle fleet

The vehicles were parked in a garage where ambient temperature was controlled to be 12°C so the temperature in the vehicles has never been lower than 0°C during experimentation.

2.2. Database presentation

The fleet monitoring led to create a database that store more than 1500 real driving cycles. This database can be used to analyze the dynamic behavior with respect to the operating conditions and investigate their effects. In this study the data used to analyze the dynamic behavior are physical measurable variables : battery current (I), the battery cell voltage ($Vcell$) and the battery module temperature (T). In addition, some characterizations have been performed on one battery pack at the beginning of the Mobypost project to measure OCV and to estimate battery capacity with constant charge/discharge profiles and internal resistance with HPPC profiles.

Figure 2 draws an example of data recorded during a driving cycle with the vehicle in pure electric mode (fuel cell stopped). Negative current values refer to currents provided to the motors, and positive current values refer to energy recovery during breaking.

The Table 1 highlights the features of the fleet after three years of experimentation exposing: determined cycle number that the batteries suffered [44], number of post delivery that the vehicle realized, distance traveled by the vehicles and the total electric charge supplied by the batteries.

It is worth noting that battery packs of vehicles were over-sized and that all the vehicles were recharged after each postal delivery. In this context, no driving cycle reached a battery state of charge value below 50%.

Table 1: fleet features

Vehicle number	Battery cycle number	Postal delivery number	Distance traveled (km)	Electric charge supplied (Ah)
1	74	160	2600	7913
2	83	203	2950	8816
3	69	154	2320	7640
4	89	243	3200	9600
5	76	145	1980	8015
6	39	110	1500	4184
7	62	149	2140	6579
8	83	188	3016	9354
9	60	159	1925	6133
10	69	171	2176	6860

3. ECM and parameters identification

3.1. ECM structure

Electrical circuit model are commonly used to reproduce the temporal battery voltage response. Several structures of equivalent circuits can be found in the litterature but a very common is highlighted in Figure 3 [40, 45, 46]. By integrating R//C circuits, this simple structure allows reproducing the dynamic behavior and the voltage response of a battery which is composed of transient periods of different durations. Therefore, the R//C circuits time constants (τ) will be different so that the model is able to reproduce different time order responses. R//C circuits are used to represent impedances linked to the charge transfer effects, double layer effects, diffusion and relaxation phenomena. The number of R//C integrated in the model refers to the desired accuracy and computing time limitations. Models can be found considering only one R//C circuit as in [13, 47–49], or two R//C circuits [38, 39, 50, 51], or with three R//C circuits [52–54].

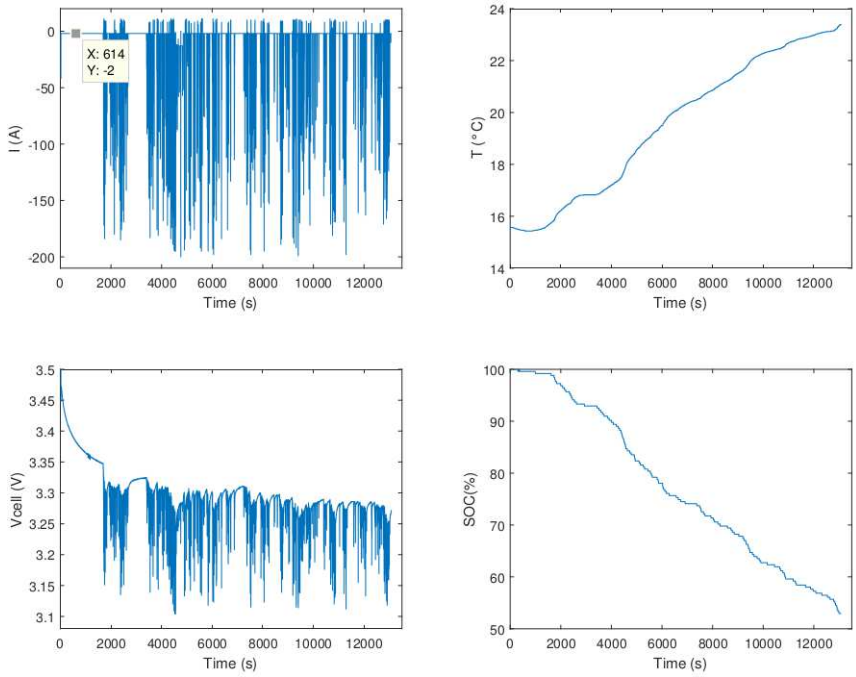

Figure 2: Data measured during a postal delivering

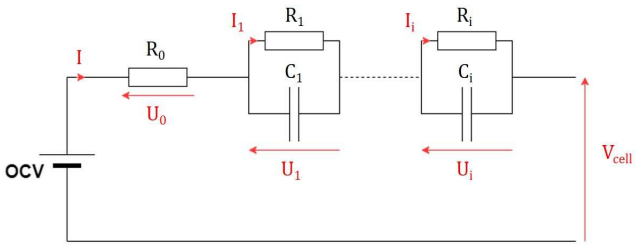

Figure 3: Battery RC model

In the proposed study the equivalent circuit integrates three R//C circuits in order to approach a good compromise between accuracy and computational requirements. Theoretically an infinite number of R//C circuits would be necessary to represent the complete voltage response but practically increasing the number of R//C circuits will proportionally increase the number of parameters of the model and consequently the computational requirements. In the proposed structure, three R//C circuits are used to represent the double layer effects, charge transfer phenomena, diffusion phenomena and relaxation phases according to the following distinction.

The model of Figure 3 contains parameters corresponding to resistances and capacitors:

- A resistance R_0 representing the ohmic losses related to the physical nature of the electrodes and the electrolyte.
- A first R//C circuit linked to the effects of the double layer capacity and charge transfer phenomena. The time constant will be the smallest of the model.
- Two R//C circuits linked to the diffusion phenomenon in the electrolyte and the relaxation phases. Time constants of these circuits will be higher.

3.2. Parameter identification

A large number of methods has been presented during the last decades to identify battery model parameters. The recursive least square and the Kalman filter are the most common because of their low complexity. Zhou et al. [55] proposed a method based on recursive least square algorithm to identify parameters of a one R//C circuit ECM. Results show satisfying accuracy but the method is tested with a simplified HPPC profile and variations of ambient conditions are not considered. Ren et al. [41] used a Kalman filter to estimate the parameters of an ECM and to estimate the SOC. Based on the model and the SOC estimation the battery capacity can be quantified. Temperature variations are not considered and simulation and validation have been performed on simplified HPPC profiles which may not fully reflect actual operating conditions.

Zhang et al. [42] assured that the accuracy of such adaptative methods is generally not satisfying. The authors preferred to use optimization algorithm in order to identify ECM parameters. In their study, they proposed an ECM based method to reproduce the dynamic behavior of a battery pack and estimate its capacity. Firstly the optimization algorithm was applied to identify ECM parameters, then a particle filter was used to estimate the SOC and finally a recursive least square algorithm was performed to quantify the battery capacity. Results showed satisfying accuracy. However, the method was tested on lab with simplified HPPC profile and temperature variations were not considered.

Considering the previous study [42], the use of an optimization algorithms have been also preferred in our study as the feature of more effective in parameters identification. In a different approach, our contribution is here to build a reliable battery model able to reproduce the dynamic behavior during actual driving cycle with good accuracy by using data directly issued from a vehicle monitoring. Moreover, the model will be reliable regardless of varying operating conditions.

3.3. Model equations

The first step is to define the model equations and the mathematical relationships linking ECM parameters to operating conditions. From

Figure 3, the equation governing the battery cell output voltage during discharge are given by:

$$V_{cell_{estimated}} = OCV - U_0 - U_1 - ... - U_i \quad (1)$$

OCV being the Open Circuit Voltage.

$$\frac{dU_i}{dt} = \frac{1}{C_i}.I - \frac{1}{R_i.C_i}.U_i \quad (2)$$

Solving the first order differential equation (2) leads to the following expression (3). It is worth noting that the acquisition frequency is $1Hz$, so $\boldsymbol{t}$ is discretized with a sampling period of 1s to solve the equation.

$$U_i(n) = U_i(n-1).e^{\frac{-(t(n)-t(n-1))}{R_i.C_i}} + R_i.(1 - e^{\frac{-(t(n)-t(n-1))}{R_i.C_i}}).I(n) \quad (3)$$

R_i and C_i being the resistive and capacitive parameters of the electrical equivalent circuit given in Figure 3.

In order to integrate thermal dependency to the model, resistive parameters will be dependent on the temperature as in (4). This equation form was prefered because of the temperature dependence following an Arrhenius law [56] and was demonstrated in [57],[58] or in [59] based on experiments.

$$R_i(n) = a_i.exp(b_i.T(n)) + c_i \quad (4)$$

where a_i , b_i and c_i are constants to be identified. T is the temperature in Celsius degree.

As presented in [60], battery internal resistance is also dependent on the SOC value. The relationship is exponential, the lower the state-of-charge, the higher the resistance. However, for a state of charge higher than 0.3, the internal resistance remains constant. In this study, driving profiles never reach SOC values lower than 0.3, consequently this relationship has not been considered in the proposed model.

Concerning the OCV, it is known that the latter is a measure of the battery electromotive force which have a monotonic relationship with the battery SOC [57, 61]. Therefore, accurate knowledge of this non-linear relationship is required for adaptive SOC estimation throughout the use of the battery. Equally, relationship between the OCV and the temperature of the battery cells has been proven [62, 63]. The consequence is a variation of the usable battery capacity [64]. Therefore, to better reproduce the battery dynamic behavior, both relationships have to be considered in the proposed model.

For this purpose, OCV characterizations have been performed in order to translate mathematically its evolution with respect to the temperature and the SOC. It is worth noting that, as highlighted on the Figure 2, when the vehicle is stopped (speed = 0) ancillaries require a constant current of 2A. To fit with this application, the choice was made to characterized pseudo OCV by measuring discharge curves at very low current (C/22). Figure 4 highlights three pseudo OCV evolutions measured at three different temperatures. As shown in Figure 4, a decomposition of each part of the curves allowed to identify mathematical expressions able to reproduce the path of the curves. For example, it can be noticed that the OCV value decreases exponentially when the temperature decreases. Mathematically, this phenomenon is governed by the expression $\alpha.exp(\beta.T(t))$.

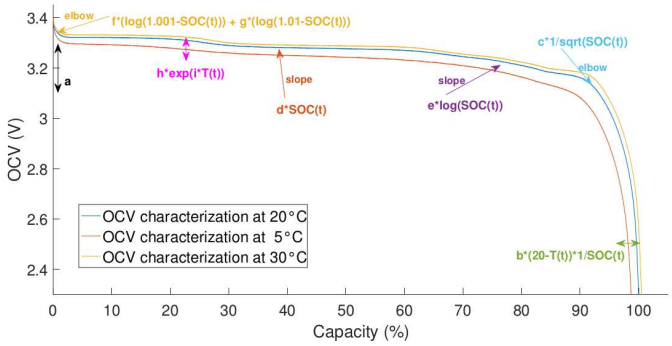

Figure 4: OCV mathematical function decomposition

The deduced empiric mathematical function (5) can be used to reproduce OCV evolution according to the temperature and SOC. Parameters *a, b, c, d, e, f, g, h* and *i* are constants to be identified. Based on the measured operating data, the parameter identification allows to adjust the OCV evolution path specific to each $LiFePO_4$ cell. Consequently, OCV of a $LiFePO_4$ cell can be estimated online without further characterizations.

$$\begin{aligned} OCV(t) = a + \frac{b.(20 - T(t))}{SOC(t)} + \frac{c}{sqrt(SOC(t))} + d.SOC(t) \\ + e.ln(SOC(t)) + f.ln(1.001 - SOC(t)) \\ + g.ln(1.01 - SOC(t)) + h.exp(i.T(t)) \end{aligned} \quad (5)$$

T is the temperature in Celsius degree.

3.4. State of charge reference

As the battery SOC is an input of the proposed model, a reference value is required to identify ECM parameters. Coulomb counting is a common method to estimate the SOC easily [10]. The SOC could be computed with equation (6).

$$SOC(t) = SOC(0) - \frac{1}{Q_{batt} \times 3600} \int_0^t I.dt \quad (6)$$

where Q_{batt} represents the battery capacity in Ah.

However, this method can be inaccurate as the battery capacity varies with respect to the temperature, as exposed in Figure 4, the aging and the current [11]. To determine a good SOC reference, we need a relationship between the capacity and the temperature. This would enable to adjust the battery capacity in (6). Based on characterizations which aimed at measuring the battery capacity under three different temperatures (2°C, 20°C, 30°C), the empirical relationship (7) was determined with a polynomial regression.

$$Q_{batt} = -0.025 \times T^2 + 1.6 \times T + 86.76 \quad (7)$$

where T is the temperature in Celsius degree. Figure 5 illustrates this empiric relationship. The nominal capacity is $110Ah$ at 23°C for a discharge current of C/5.

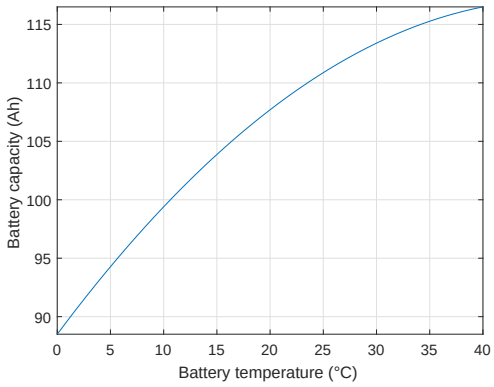

Figure 5: Characterized battery capacity versus temperature

3.5. Optimization algorithm

Optimization methods can be summarized as identifying a set of input parameters (x_n) minimizing a mathematical function f(x_n). The nature is a great inspiration for proposing optimization methods such as Genetic Algorithms, Ant Colony System, Simulated Annealing, Particle Swarm Optimization or again big-bang big-crunch [65–67]. Optimization algorithms have been already used to identify parameters of a battery model [42, 68]. The purpose is to identify the set of input parameters model minimizing the objective function. In this case the objective function to minimize is the Normalized Root Mean Square Error (NRMSE) (8).

$$NRMSE = \frac{RMSE}{max(Vcell_{real}) - min(Vcell_{real})} \tag{8}$$

where RMSE is the Root Mean Square Error, $max(Vcell_{real}$ is the real cell voltage maximum value, $min(Vcell_{real}$ is the real cell voltage minimum value.

In this work the Big-Bang Big-Crunch (BB-BC) algorithm has been prefered as it presents good results and performances in [69]. It is worth noting that in this study the purpose is not to demonstrate which optimization algorithm is the best. The proposed BB-BC algorithm refers to one of the theories of the universe evolution [69, 70]. This theory, explains that the universe expansion phase due to the big bang will end and will be replaced by a universe contraction phase named big crunch.

The BB-BC algorithm is constituted by the following steps:

- **Step 1:** create an initial population of N_{pop} candidates randomly, respecting the search space limitations.
- **Step 2:** evaluate performance of each candidate by applying the objective function.
- **Step 3:** identifying the best candidate (named center of mass). Candidate leading to the lowest error.
- **Step 4:** create a new population around the center of mass and reduce the search space. However an exploration probability is preserved to get out of a possible local minimum: some candidates are created in the entire search space looking for a global optimum.
- **Step 5:** return to step 2 while stopping criteria is not met.

The reduction of the search space is represented by a function inversely proportional to the number of generation. The equation (9) illustrates the research space division (RS_{div}) according to the number of generations (gen):

$$RS_{div}(gen) = \frac{1}{gen} \tag{9}$$

This function radically reduces the search space for the first generations which can lead to progress to a local minimum instead of the desired global minimum. In order to tackle this issue, another way to reduce the search space, proposed in [69], has been used in this study. The proposed method divides more slowly the search space during first generations and then accelerates to find the results more efficiently. For this purpose, an exponential function replaces the linear function in the proposed version of the algorithm.

3.6. Training data

To improve robustness of the model and avoid extrapolations, identifying model parameters according to the entire operating range is of particular importance. For that purpose, four driving cycles (cf. Figure 7) have been chosen as they have been realized at four different temperatures as detailed below. The entire operating temperature range of the vehicle is therefore considered (from 1°C to 25°C).

- Cycle 1 : average temperature 3°C
- Cycle 2 : average temperature 7°C
- Cycle 3 : average temperature 18°C
- Cycle 4 : average temperature 24°C

3.7. Modeling results

As a result of the parameters identification, the Figure 6 draws a comparison between the estimated and the measured voltage during the driving cycle 3 used for model building. It is worth remembering that this voltage is the result of a parallel association of single LFP cells which reach a capacity of 110Ah. Results highlight the good accuracy of the model. The obtained error is $NRMSE = 0.016$. The model is able to provide an accurate cell voltage estimation with respect to the temperature and the SOC. Tables 2 and 3 present the values of the identified model parameters. Three different time constants are obtained: 2 seconds to reproduce the end of charge transfer and double layer effects and the beginning of diffusion phenomena, 40 seconds and 400 seconds to reproduce both diffusion phenomena and relaxation phases. The efficiency could be improved by adding others R//C circuits with higher time constants up to several hours in order to reproduce relaxation phenomena at best [71]. Figure 8 illustrates the evolution of the internal resistance *Rin* with respect to the temperature. In this study *Rin* is defined as the sum of the four resistive parameters. Figure 9 compares OCV estimation based on operating data and OCV measures from characterization.

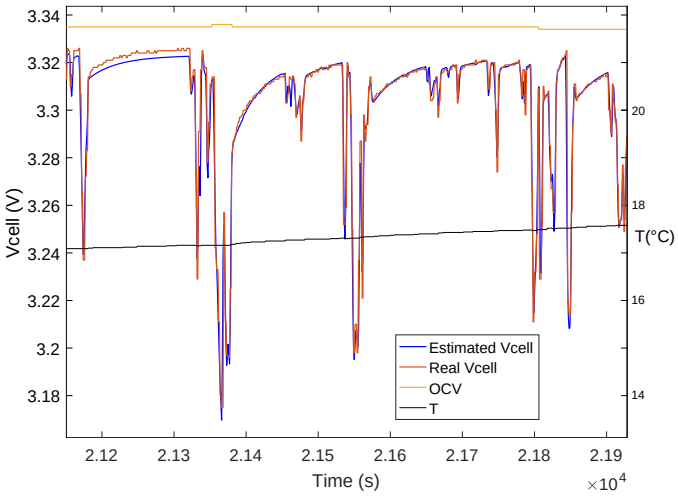

Figure 6: Cell voltages comparison with a driving cycle used for parameters identification

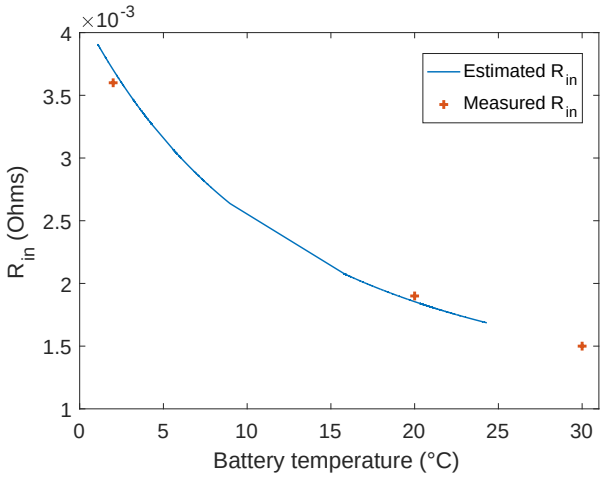

Figure 8: Internal resistance evolution versus temperature

Table 2: Model parameters for $T = 20°C$

Model parameter	Value
τ_1	$2\ s$
τ_2	$40\ s$
τ_3	$409\ s$
C_1	$1266F$
C_2	$47772F$
C_3	$454800F$
a	$3.566\ V$
b	$-1.013 \times 10^{-4}\ V°C^{-1}$
c	$-0.0700\ V$
d	$0.0735\ V$
e	$-0.0191\ V$
f	$-0.0744\ V$
g	$0.0657\ V$
h	$-0.023\ V$
i	$-0.00201\ °C^{-1}$

Table 3: Model resistive parameters

Model element	$a_i(m\Omega)$	$b_i(°C^{-1})$	$c_i(m\Omega)$
R_0	0.407	−0.067	0.145
R_1	0.678	−0.058	0.305
R_2	0.889	−0.04	0.186
R_3	1.1	−0.14	0.427

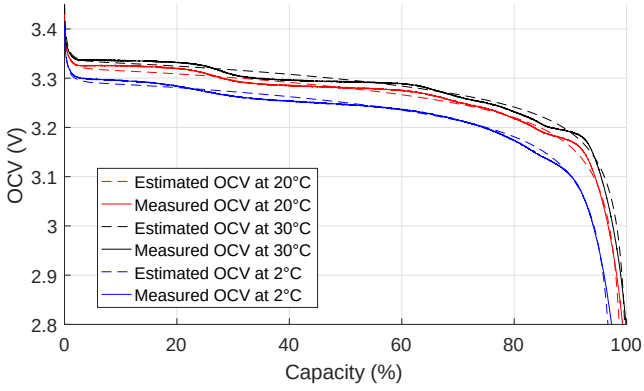

Figure 9: Comparison between estimated and measured OCV at three different temperatures

Then, the model must be validated by verifying its accuracy for an input profile (current and temperature) different from one used for parameters identification. Thereby, Figure 10 compares both estimated and real voltage responses for a driving cycle selected randomly from the database. The battery temperature range is from $13°C$ to $17°C$. The error is $NRMSE = 0.02$ which proves the validity of the proposed model.

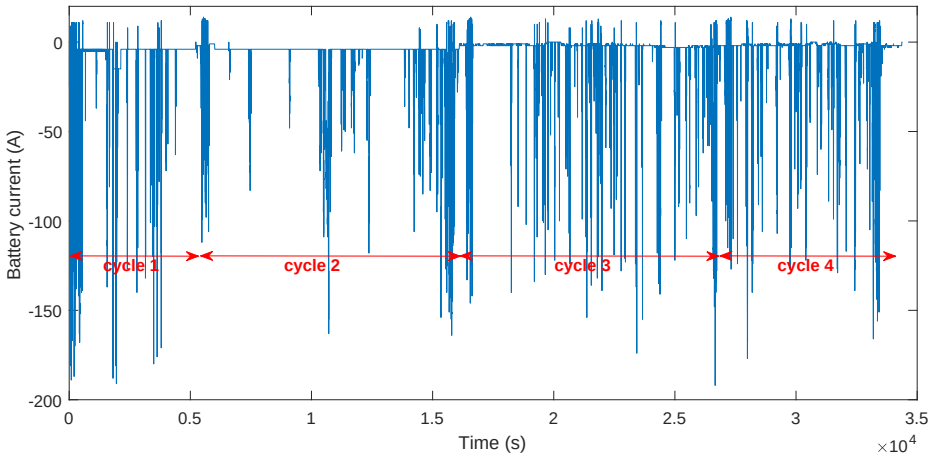

Figure 7: Driving cycles used for parameter identification

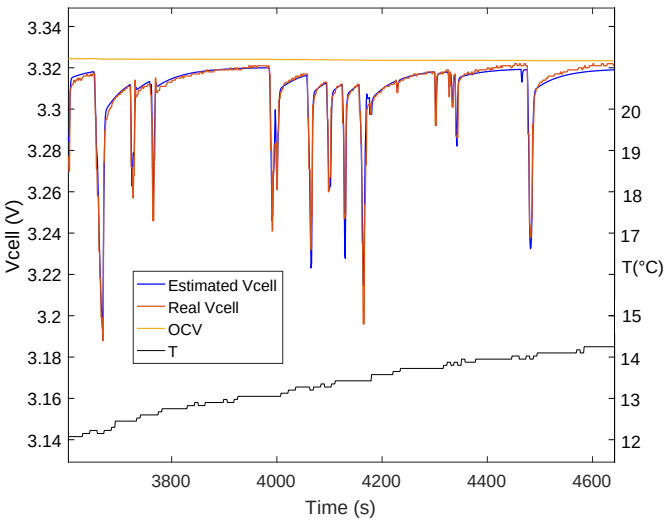

Figure 10: Cell voltages comparison with entire driving cycle used for validation

In this section, a method has been proposed to model a battery with respect to temperature and SOC dependencies. This method allows to estimate the cell voltage response with a good accuracy whatever the operating conditions.

4. On board estimation of SOH indicators

The previous parameter identification could be applied during the vehicle lifetime to follow model parameters evolution according to the aging. In particular, the internal resistance *Rin* evolution can be dissociated from the temperature influence. Consequently, SOH referring to power fade, could be quantified on-board all along the vehicle operation. However, the proposed modeling method needs to know the value of the SOC (cf. equation (5)) and SOC is directly depending on battery capacity. Therefore monitoring this capacity is a key for on board estimation of SOH indicators (internal resistance and capacity).

As mentioned before, the capacity varies with respect to the temperature, the current and the aging. The coulomb counting is a simple method but not sufficient for a good estimation in embedded applications. This study proposes a method to estimate simultaneously the battery SOC and the battery capacity based on the previous presented model.

The proposed approach to estimate the usable battery capacity is based on SOC variations (ΔSOC) and electric charge variations ΔQ (in Ah). The battery capacity is defined by the expression (10).

$$Qbatt_{estimated} = \frac{\Delta Q}{\Delta SOC} \tag{10}$$

In this case, as ΔSOC is at the denominator of the expression (10), a small ΔSOC will easily lead to oscillations. This is why it is advisable to consider sufficiently large SOC variations to minimize estimation errors. In the proposed method, ΔSOC is defined as the difference between the SOC at time k and the initial SOC, so the estimation will be more accurate through the time steps.

The proposed approach is governed by the following **algorithm 1**. All along a driving cycle, measures are acquired at a sampling period Δt. At each time step, the sum of supplied current is computed and stored in variable *int*. With this sum, the quantity of electric charges ΔQ (in Ah) delivered by the battery can be determined. Finally, estimated capacity is determined by the ratio between ΔQ and ΔSOC.

Algorithm 1 Capacity estimation

while $k < end$ **do**
  $int = int + I(k)$
  $\Delta Q(k) = int.\Delta t/3600$
  $\Delta SOC(k) = SOC(0) - SOC(k)$
  $Qbatt_{estimated}(k) = \frac{\Delta Q(k)}{\Delta SOC(k)}$
  $k = k + 1$
end while

Then, the first step is to propose an SOC estimation. Several methods have been exposed in the literature to estimate battery SOC such as artificial neural networks [72, 73], Kalman filters, particle filter, recursive least square or again fuzzy logic. Considering the literature, Kalman filtering is certainly the most common method to estimate

SOC due to its good accuracy, low computational requirement and easy implementation [47, 74–76]. For theses reasons a Kalman filter based method has been preferred in this study.

4.1. Extended Kalman Filter equations

Kalman Filters (KF) can be used to estimate a system state which cannot be directly measured, in this case the battery state of charge. The Extended Kalman Filter (EKF) is a variant of the basic Kalman Filter which is usable only if the system is linear. EKF is one of the commonly used methods for battery parameter and state estimation [47, 76]. This filter is a recursive algorithm that combines a model which is used to estimate a measurable value and a measurement data set to seek for an optimal estimation of the internal state of the system. Once a new measurement is available, the prediction error is used to correct the state prediction. A good detailed introduction on the EKF and its applications for SOC estimation has been provided in [74]. EKF relies on two functions : a state equation (11) and a measurement equation (12). These two equations are governed by the nonlinear vector functions f and h, where x_k is the state vector at time index k, u_k is the system input, w_k is the process noise, y_k is the output of the system and v_k is the measure noise that affects the measurement of the output.

$$x_k = f(x_{k-1}, u_{k-1}) + w_k \tag{11}$$

$$y_k = h(x_k, u_k) + v_k \tag{12}$$

The function f can be used to compute the predicted state from the previous estimate and the function h can be used to compute the predicted output from the predicted state. As KF cannot work in a nonlinear model, functions f and h cannot be applied directly so a linearized process method is required for EKF. State equation (11) and measurement equation (12) are linearized iteratively by Taylor series expansion. The Jacobian matrices of the first order Taylor expansion are computed as in (13) and (14). F_k and H_k are the first partial derivative matrices of functions f and h with respect to x_k.

$$F = \frac{\partial f(x_k, u_k)}{\partial x_k} \tag{13}$$

$$H = \frac{\partial h(x_k, u_k)}{\partial x_k} \tag{14}$$

The filter consists of two phases : one for predicting the measured value and one for correcting. The prediction phase is governed by the two following equations (15) and (16) :

Prediction of the state variable at time k :

$$\widehat{x_k^-} = f(\widehat{x}_{k-1}, u_{k-1}) \tag{15}$$

Prediction of covariance error :

$$P_k^- = F_k.P_{k-1}.F_k^T + Q_k \tag{16}$$

And the measurements update equations are governed by (17)-(20):

Update of innovation covariance :

$$S_k = H_k.P_k^-.H_k^T + R_k \tag{17}$$

Update of Kalmain gain :

$$K_k = P_k^-.H_k^T.S_k^{-1} \tag{18}$$

Optimal estimation of system state at time k :

$$\widehat{x_k} = \widehat{x^-} + K_k.(y_k - \widehat{y}_k) \tag{19}$$

Update of system state error covariance matrix :

$$P_k = (I - K_k.H_k).P_k^- \tag{20}$$

Q_k and R_k are the covariances of the process and measurement noises. P_k is the a posteriori covariance matrix which is a measure of the estimated accuracy of the state estimation.

To apply EKF, the first step is to transform the SOC expression (6) to a discrete form (21):

$$SOC(k) = SOC(k-1) - I(k).\frac{\Delta t}{Qbatt_{estimated} \times 3600} \tag{21}$$

With $Qbatt_{estimated}$ the usable battery capacity estimation obtained through the **Algorithm 1**.

The Kalman filter state equation $f(x_k, u_k)$ (11) and measurement equation $h(x_k, u_k)$ (12) can now be expressed respectively as in (22) and (23).

$$\begin{bmatrix} SOC_{k+1} \\ U_{1_{k+1}} \\ U_{2_{k+1}} \\ U_{3_{k+1}} \end{bmatrix} = \begin{bmatrix} SOC_k - I(k).\dfrac{\Delta_t}{Qbatt} \\ U_{1_k}.e^{\frac{-\Delta t}{R_1.C_1}} + R_1.(1 - e^{\frac{-\Delta t}{R_1.C_1}}).I_k \\ U_{2_k}.e^{\frac{-\Delta t}{R_2.C_2}} + R_2.(1 - e^{\frac{-\Delta t}{R_2.C_2}}).I_k \\ U_{3_k}.e^{\frac{-\Delta t}{R_1.C_1}} + R_3.(1 - e^{\frac{-\Delta t}{R_3.C_3}}).I_k \end{bmatrix} \tag{22}$$

$$h(x_k, u_k) = \begin{bmatrix} OCV_k & -U_{1_k} & -U_{2_k} & -U_{3_k} & -R_{0_k}.I_k \end{bmatrix} \tag{23}$$

with the battery current defined as the input signal $u_k = I_k$. Jacobian matrices F_k and H_k can be expressed respectively as in (24) and (25) :

$$F_k = \frac{\partial f(x_k, u_k)}{\partial x_k} = \begin{bmatrix} 1 & 0 & 0 & 0 \\ 0 & e^{\frac{-\Delta t}{R_1.C_1}} & 0 & 0 \\ 0 & 0 & e^{\frac{-\Delta t}{R_2.C_2}} & 0 \\ 0 & 0 & 0 & e^{\frac{-\Delta t}{R_3.C_3}} \end{bmatrix} \tag{24}$$

$$H_k = \frac{\partial h(x_k, u_k)}{\partial x_k} = \begin{bmatrix} \dfrac{\partial OCV}{\partial SOC} \\ -1 \\ -1 \\ -1 \end{bmatrix}^T \tag{25}$$

4.2. EKF estimation of SOC and capacity

Figures 11, 12 and 13 highlight SOC estimation with the proposed EKF. The figures compare the EKF estimation and a basic coulomb counting during three driving cycles realized at three different temperatures : 20°C, 5°C and 25°C. These cycles have been selected in the database in order to represent the full temperature range in which the driving cycles were realized. The Figure 11 highlights two SOC estimations compared to a coulomb counting for two driving cycles realized at 20°C. It can be seen that both estimations achieve same SOC final value than the coulomb counting regardless of the final state of charge value. For a temperature of 5°C (cf. Figure 12), the estimation differs from the coulomb counting as the usable battery capacity changed due to temperature variation. In the third case of 25°C (cf. Figure 13), the difference is less visible. Kalman filter estimation remains close to the coulomb counting as at higher temperatures the variation of usable capacity is less significant (cf. Figure 5). This shows that the proposed estimation is able to consider battery capacity variations. To verify the proposed method, SOC estimations in Figures

12 and 13 have been compared with coulomb counting reference performed with the characterized battery capacity at both temperatures. This way, it can be seen that estimations from the Kalman filter consider battery capacity decreasing due to the low temperature and small capacity increasing due to higher temperature which is faithful to characterizations.

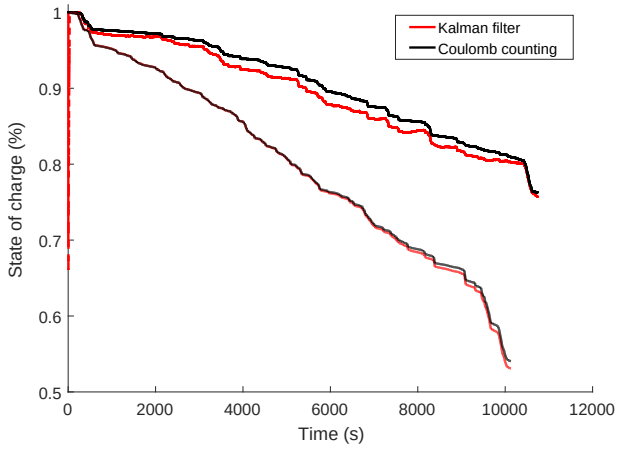

Figure 11: State of charge estimation for battery temperature at 20°C

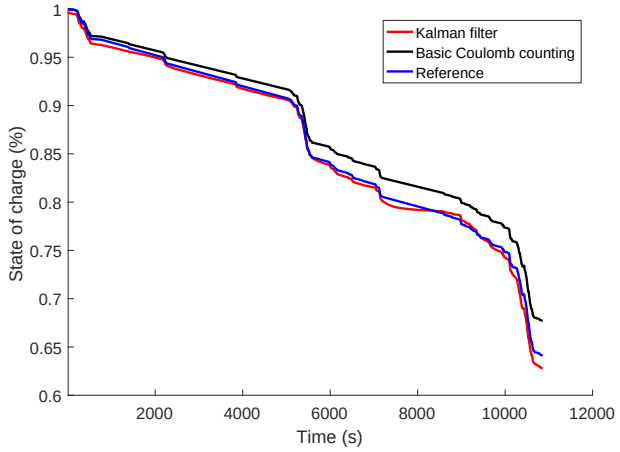

Figure 12: State of charge estimation for battery temperature at 5°C

Results above show that the Kalman filter is able to concurrently estimate the state of charge and the battery usable capacity. The estimation of the battery capacity is an important challenge as it is directly linked to the vehicle autonomy and is not constant during the battery lifetime. That is why the method for SOC estimation needs to be robust regarding the knowledge of the real value of capacity. This is thus mandatory to verify that SOC estimation remains reliable whatever the knowledge of the battery capacity. For that purpose the previous presented method has been performed with two different capacity values initialized in the algorithm. The Figure 14 highlights the proposed SOC estimation at 20°C and compare it with a basic coulomb counting initialized with two different initial capacity value. As expected, the coulomb counting estimations differ as the capacity values in the SOC expression (cf. equation (6)) are different. In contrary, the value

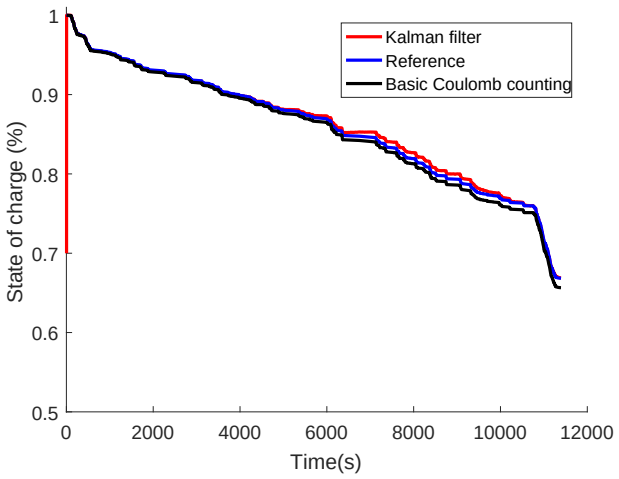

Figure 13: State of charge estimation for battery temperature at 25°C

of the initial capacity *Qbatt* in the Kalman filter state equation (21) does not affect the SOC estimation. Indeed, even if the initial capacity value is different (210 *Ah* instead of 110 *Ah*), the SOC estimation converges to the same value. The proposed method corrects the battery capacity value and does not require to further measure the real value to provide a reliable SOC estimation.

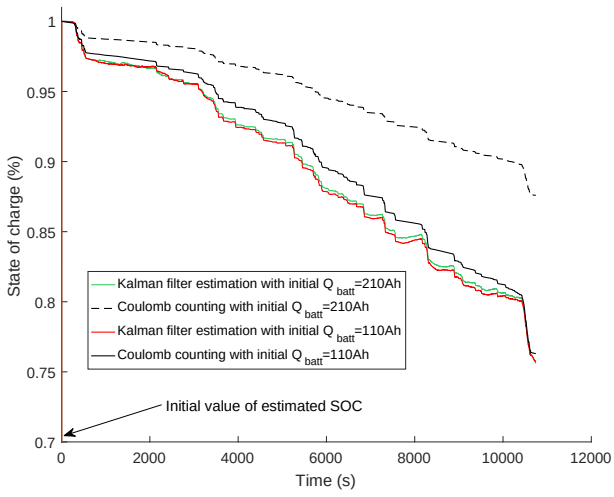

Figure 14: State of charge estimation with two different initial capacities

The proposed approach can be applied on-board all along the vehicle lifetime coupled with ECM parameters identifications to estimate the battery state of charge and capacity, which directly refers to SOH indicator, depending on the temperature and the battery aging. Contrary to the initial estimation (cf. section 3.4) this EKF estimation is based on battery model. Therefore, if model parameters vary with the aging, the battery SOC and usable capacity can be concurrently estimated based on these new parameters. In this way aging will be considered.

5. Conclusion

Based on vehicle operating only, this paper proposed a method to identify state of health indicators of a $LiFePO_4$ battery cell: available capacity and internal resistance referring to the available power. The method is based on an electrical circuit model to reproduce and simulate battery dynamic behavior according to operating conditions. The proposed model is able to reproduce the battery dynamic behavior: cell voltage with respect to thermal and state of charge dependencies, with a very promising accuracy. Model parameters can be used to estimate the internal resistance which is a first state of health indicator. Based on a Kalman filter, the model can then be used to estimate concurrently the state of charge and the available capacity, which is a second state of health indicator, considering the temperature variations and the aging. The proposed method could be integrated on board and applied during the entire vehicle lifetime to provide a reliable state of charge estimation and to follow state of health in order to contribute to a better understanding of the degradation laws and to develop better energy management strategies.

Otherwise, future aging data will be generated to extend the database in order to validate the proposed method, to analyze battery state of health evolution and to study effects of actual operating conditions on the battery degradation.

6. Acknowledgement

This research work was funded by the region of Bourgogne Franche-Comté, France.

7. References

[1] M. H. Lipu, M. Hannan, A. Hussain, M. Hoque, P. J. Ker, M. Saad, A. Ayob, A review of state of health and remaining useful life estimation methods for lithium-ion battery in electric vehicles: Challenges and recommendations, Journal of Cleaner Production 205 (2018) 115–133.

[2] C. M. Martinez, X. Hu, D. Cao, E. Velenis, B. Gao, M. Wellers, Energy Management in Plug-in Hybrid Electric Vehicles: Recent Progress and a Connected Vehicles Perspective, IEEE Transactions on Vehicular Technology 66 (6) (2017) 4534–4549.

[3] Y. Han, Q. Li, T. Wang, W. Chen, L. Ma, Multisource coordination energy management strategy based on SOC consensus for a PEMFC-battery-supercapacitor hybrid tramway, IEEE Transactions on Vehicular Technology 67 (1) (2018) 296–305.

[4] L. H. Saw, Y. Ye, A. A. Tay, Integration issues of lithium-ion battery into electric vehicles battery pack, Journal of Cleaner Production 113 (2016) 1032–1045.

[5] M. Dubarry, B. Y. Liaw, M.-S. Chen, S.-S. Chyan, K.-C. Han, W.-T. Sie, S.-H. Wu, Identifying battery aging mechanisms in large format Li ion cells, Journal of Power Sources 196 (7) (2011) 3420–3425.

[6] N. El Ghossein, A. Sari, P. Venet, Degradation behavior of Lithium-Ion Capacitors during calendar aging, in: 2017 6th International Conference on Renewable Energy Research and Applications, ICRERA 2017, Vol. 2017-January, Institute of Electrical and Electronics Engineers Inc., 2017, pp. 142–146.

[7] A. El Mejdoubi, H. Gualous, H. Chaoui, G. Alcicek, Experimental investigation of calendar aging of lithium-ion batteries for vehicular applications, in: 2017 4th International Electromagnetic Compatibility Conference, EMC Turkiye 2017, Institute of Electrical and Electronics Engineers Inc., 2017.

[8] C. R. Birkl, M. R. Roberts, E. McTurk, P. G. Bruce, D. A. Howey, Degradation diagnostics for lithium ion cells, Journal of Power Sources 341 (2017) 373–386.

[9] A. Barré, B. Deguilhem, S. Grolleau, M. Gérard, F. Suard, D. Riu, A review on lithium-ion battery ageing mechanisms and estimations for automotive applications, Journal of Power Sources 241 (2013) 680–689.

[10] M. Berecibar, I. Gandiaga, I. Villarreal, N. Omar, J. Van Mierlo, P. Van den Bossche, Critical review of state of health estimation methods of Li-ion batteries for real applications, Renewable and Sustainable Energy Reviews 56 (2016) 572–587.

[11] R. Xiong, L. Li, J. Tian, Towards a smarter battery management system_ A critical review on battery state of health monitoring methods, Journal of Power Sources 405 (2018) 18–29.

[12] L. Zheng, J. Zhu, D. D.-C. Lu, G. Wang, T. He, Incremental capacity analysis and differential voltage analysis based state of charge and capacity estimation for lithium-ion batteries, Energy 150 (2018) 759–769.

[13] A. Guha, A. Patra, State of Health Estimation of Lithium-Ion Batteries Using Capacity Fade and Internal Resistance Growth Models, IEEE Transactions on Transportation Electrification 4 (1) (2017) 135–146.

[14] K. S. Ng, C.-S. Moo, Y.-P. Chen, Y.-C. Hsieh, Enhanced coulomb counting method for estimating state-of-charge and state-of-health of lithium-ion batteries, Applied Energy 86 (9) (2009) 1506–1511.

[15] Z. Guo, X. Qiu, G. Hou, B. Y. Liaw, C. Zhang, State of health estimation for lithium ion batteries based on charging curves, Journal of Power Sources 249 (2014) 457–462.

[16] C. Weng, J. Sun, H. Peng, A unified open-circuit-voltage model of lithium-ion batteries for state-of-charge estimation and state-of-health monitoring, Journal of Power Sources 258 (2014) 228–237.

[17] D. Andre, M. Meiler, K. Steiner, H. Walz, T. Soczka-Guth, D. Sauer, Characterization of high-power lithium-ion batteries by electrochemical impedance spectroscopy. II: Modelling, Journal of Power Sources 196 (12) (2011) 5349–5356.

[18] M. Galeotti, L. Cinà, C. Giammanco, S. Cordiner, A. Di Carlo, Performance analysis and SOH (state of health) evaluation of lithium polymer batteries through electrochemical impedance spectroscopy, Energy 89 (2015) 678–686.

[19] M. Swierczynski, D. I. Stroe, T. Stanciu, S. K. Kær, Electrothermal impedance spectroscopy as a cost efficient method for determining thermal parameters of lithium ion batteries: Prospects, measurement methods and the state of knowledge, Journal of Cleaner Production 155 (2017) 63–71.

[20] Y. Cui, P. Zuo, C. Du, Y. Gao, J. Yang, X. Cheng, Y. Ma, G. Yin, State of health diagnosis model for lithium ion batteries based on real-time impedance and open circuit voltage parameters identification method, Energy 144 (2018) 647–656.

[21] H. Wang, A. Gaillard, D. Hissel, A review of DC/DC converter-based electrochemical impedance spectroscopy for fuel cell electric vehicles, Renewable Energy 141 (2019) 124–138.

[22] H. Wang, A. Gaillard, D. Hissel, Online electrochemical impedance spectroscopy detection integrated with step-up converter for fuel cell electric vehicle, International Journal of Hydrogen Energy 44 (2) (2019) 1110–1121.

[23] M. Dubarry, B. Y. Liaw, Identify capacity fading mechanism in a commercial LiFePO 4 cell, Journal of Power Sources 194 (2009) 541–549.

[24] E. Riviere, A. Sari, P. Venet, F. Meniere, Y. Bultel, Innovative incremental capacity analysis implementation for C/LiFePO4 cell state-of-health estimation in electrical vehicles, Batteries 5 (2).

[25] L. Zheng, J. Zhu, D. D.-C. Lu, G. Wang, T. He, Incremental capacity analysis and differential voltage analysis based state of charge and capacity estimation for lithium-ion batteries, Energy 150 (2018) 759–769.

[26] Y. Li, M. Abdel-Monem, R. Gopalakrishnan, M. Berecibar, E. Nanini-Maury, N. Omar, P. van den Bossche, J. Van Mierlo, A quick on-line state of health estimation method for Li-ion battery with incremental capacity curves processed by Gaussian filter, Journal of Power Sources 373 (2018) 40–53.

[27] Y. Li, K. Liu, A. M. Foley, A. Zülke, M. Berecibar, E. Nanini-Maury, J. Van Mierlo, H. E. Hoster, Data-driven health estimation and lifetime prediction of lithium-ion batteries: A review, Renewable and Sustainable Energy Reviews 113 (2019) 109254.

[28] J. Wu, Y. Wang, X. Zhang, Z. Chen, A novel state of health estimation method of Li-ion battery using group method of data handling, Journal of Power Sources 327 (2016) 457–464.

[29] G.-w. You, S. Park, D. Oh, Real-time state-of-health estimation for electric vehicle batteries: A data-driven approach, Applied Energy 176 (2016) 92–103.

[30] V. Klass, M. Behm, G. Lindbergh, A support vector machine-based state-of-health estimation method for lithium-ion batteries under electric vehi-

cle operation, Journal of Power Sources 270 (2014) 262–272.
[31] Y. Deng, H. Ying, J. E, H. Zhu, K. Wei, J. Chen, F. Zhang, G. Liao, Feature parameter extraction and intelligent estimation of the State-of-Health of lithium-ion batteries, Energy 176 (2019) 91–102.
[32] S. Shen, M. Sadoughi, X. Chen, M. Hong, C. Hu, A deep learning method for online capacity estimation of lithium-ion batteries, Journal of Energy Storage 25 (2019) 100817.
[33] J. Tian, R. Xiong, W. Shen, J. Wang, R. Yang, Online simultaneous identification of parameters and order of a fractional order battery model, Journal of Cleaner Production (2019) 119147.
[34] M. Jafari, K. Khan, L. Gauchia, Deterministic models of Li-ion battery aging: It is a matter of scale, Journal of Energy Storage 20 (2018) 67–77.
[35] M. Mastali Majdabadi, S. Farhad, M. Farkhondeh, R. A. Fraser, M. Fowler, Simplified electrochemical multi-particle model for LiFePO4 cathodes in lithium-ion batteries, Journal of Power Sources 275 (2015) 633–643.
[36] J. Li, Y. Cheng, M. Jia, Y. Tang, Y. Lin, Z. Zhang, Y. Liu, An electrochemicalthermal model based on dynamic responses for lithium iron phosphate battery, Journal of Power Sources 255 (2014) 130–143.
[37] R. Gu, P. Malysz, H. Yang, A. Emadi, On the suitability of electrochemical-based modeling for lithium-ion batteries, IEEE Transactions on Transportation Electrification 2 (4) (2016) 417–431.
[38] M. Bahramipanah, D. Torregrossa, R. Cherkaoui, M. Paolone, Enhanced Equivalent Electrical Circuit Model of Lithium-Based Batteries Accounting for Charge Redistribution, State-of-Health, and Temperature Effects, IEEE Transactions on Transportation Electrification 3 (3) (2017) 589–599.
[39] P. Shen, M. Ouyang, L. Lu, J. Li, X. Feng, The co-estimation of state of charge, state of health, and state of function for lithium-ion batteries in electric vehicles, IEEE Transactions on Vehicular Technology 67 (1) (2018) 92–103.
[40] H. Chaoui, H. Gualous, Online parameter and state estimation of lithium-ion batteries under temperature effects, Electric Power Systems Research 145 (2017) 73–82.
[41] H. Ren, Y. Zhao, S. Chen, T. Wang, Design and implementation of a battery management system with active charge balance based on the SOC and SOH online estimation, Energy 166 (2019) 908–917.
[42] X. Zhang, Y. Wang, C. Liu, Z. Chen, A novel approach of battery pack state of health estimation using artificial intelligence optimization algorithm, Journal of Power Sources 376 (2018) 191–199.
[43] A. Ravey, S. Faivre, C. Higel, F. Harel, A. Djerdir, Energy management of fuel cell electric vehicle with hydrid tanks, IECON Proceedings (Industrial Electronics Conference) (2014) 3962–3967.
[44] L. Vichard, A. Ravey, S. Morando, F. Harel, P. Venet, S. Pelissier, D. Hissel, Battery aging study using field use data, in: IEEE Vehicle Power and Propulsion Conference (VPPC), 2017.
[45] J. Jiang, Y. Liang, Q. Ju, L. Zhang, W. Zhang, C. Zhang, An Equivalent Circuit Model for Lithium-sulfur Batteries, Energy Procedia 105 (2017) 3533–3538.
[46] A. Lievre, A. Sari, P. Venet, A. Hijazi, M. Ouattara-Brigaudet, S. Pelissier, Practical online estimation of lithium-ion battery apparent series resistance for mild hybrid vehicles, IEEE Transactions on Vehicular Technology 65 (6) (2016) 4505–4511.
[47] X. Li, Z. Wang, L. Zhang, Co-estimation of capacity and state-of-charge for lithium-ion batteries in electric vehicles, Energy 174 (2019) 33–44.
[48] X. Yang, Y. Chen, B. Li, D. Luo, Battery states online estimation based on exponential decay particle swarm optimization and proportional-integral observer with a hybrid battery model, Energy (2019) 116509.
[49] M. Dubarry, B. Y. Liaw, Development of a universal modeling tool for rechargeable lithium batteries, Journal of Power Sources 174 (2) (2007) 856–860.
[50] Y. Hu, S. Yurkovich, Y. Guezennec, B. Yurkovich, A technique for dynamic battery model identification in automotive applications using linear parameter varying structures, Control Engineering Practice 17 (10) (2009) 1190–1201.
[51] M. Hu, Y. Li, S. Li, C. Fu, D. Qin, Z. Li, Lithium-ion battery modeling and parameter identification based on fractional theory, Energy 165 (2018) 153–163.
[52] Y. Cao, R. C. Kroeze, P. T. Krein, Multi-timescale parametric electrical battery model for use in dynamic electric vehicle simulations, IEEE Transactions on Transportation Electrification 2 (4) (2016) 432–442.
[53] R. C. Kroeze, P. T. Krein, Electrical battery model for use in dynamic electric vehicle simulations, in: Power Electronics Specialists Conference, 2008. PESC 2008. IEEE, IEEE, 2008, pp. 1336–1342.
[54] Y. Hu, S. Yurkovich, Y. Guezennec, B. J. Yurkovich, Electro-thermal battery model identification for automotive applications, Journal of Power Sources 196 (1) (2011) 449–457.
[55] D. Zhou, A. Ravey, F. Gao, D. Paire, A. Miraoui, K. Zhang, Online estimation of state of charge of Li-ion battery using an iterated extended Kalman particle filter, 2015 IEEE Transportation Electrification Conference and Expo, ITEC 2015.
[56] B. Y. Liaw, E. P. Roth, R. G. Jungst, G. Nagasubramanian, H. L. Case, D. H. Doughty, Correlation of Arrhenius behaviors in power and capacity fades with cell impedance and heat generation in cylindrical lithium-ion cells, Journal of Power Sources 121 (2003) 874–886.
[57] J. Jaguemont, L. Boulon, Y. Dubé, Characterization and modeling of a hybrid-electric-vehicle lithium-ion battery pack at low temperatures, IEEE Transactions on Vehicular Technology 65 (1) (2016) 1–14.
[58] N. Kim, A. Rousseau, E. Rask, Parameter Estimation for a Lithium-Ion Battery from Chassis Dynamometer Tests, IEEE Transactions on Vehicular Technology 65 (6) (2016) 4393–4400.
[59] G. Giordano, V. Klass, M. Behm, G. Lindbergh, J. Sjoberg, Model-based lithium-ion battery resistance estimation from electric vehicle operating data, IEEE Transactions on Vehicular Technology 67 (5) (2018) 3720–3728.
[60] S. Wijewardana, R. Vepa, M. H. Shaheed, Dynamic battery cell model and state of charge estimation, Journal of Power Sources 308 (2016) 109–120.
[61] B. Pattipati, B. Balasingam, G. V. Avvari, K. R. Pattipati, Y. Bar-Shalom, Open circuit voltage characterization of lithium-ion batteries, Journal of Power Sources 269 (2014) 317–333.
[62] Y. Xing, W. He, M. Pecht, K. L. Tsui, State of charge estimation of lithium-ion batteries using the open-circuit voltage at various ambient temperatures, Applied Energy 113 (2014) 106–115.
[63] N. Damay, Contribution à la modélisation thermique de packs batteries LiFePO4 pour véhicules décarbonés, Ph.d. thesis, Université de Technologie de Compiègne (2016).
[64] J. Jaguemont, L. Boulon, P. Venet, Y. Dubé, A. Sari, Lithium-Ion Battery Aging Experiments at Subzero Temperatures and Model Development for Capacity Fade Estimation, IEEE Transactions on Vehicular Technology 65 (6) (2016) 4328–4343.
[65] J. R. Koza, J. R. Koza, Genetic Programming, Encyclopedia of Computer Science and Technology.
[66] A. C. Kakas, D. Cohn, S. Dasgupta, A. G. Barto, G. A. Carpenter, S. Grossberg, G. I. Webb, M. Dorigo, M. Birattari, H. Toivonen, J. Timmis, J. Branke, H. Toivonen, A. L. Strehl, C. Drummond, A. Coates, P. Abbeel, A. Y. Ng, F. Zheng, G. I. Webb, P. Tadepalli, Ant Colony Optimization, in: Encyclopedia of Machine Learning, Springer US, Boston, MA, 2011, pp. 36–39.
[67] S. Kirkpatrick, C. D. Gelatt, M. P. Vecchi, Optimization by simulated annealing, Science 220 (4598) (1983) 671–680.
[68] R. Yang, R. Xiong, H. He, H. Mu, C. Wang, A novel method on estimating the degradation and state of charge of lithium-ion batteries used for electrical vehicles, Applied Energy 207 (2017) 336–345.
[69] S. Morando, M. C. Pera, N. Youfi Steiner, S. Jemei, D. Hissel, L. Larger, Reservoir Computing optimisation for PEM fuel cell fault diagnostic, in: IEEE Vehicle Power and Propulsion Conference (VPPC), 2017.
[70] O. K. Erol, I. Eksin, A new optimization method: Big BangBig Crunch, Advances in Engineering Software 37 (2) (2006) 106–111.
[71] A. Li, S. Pelissier, P. Venet, P. Gyan, Fast characterization method for modeling battery relaxation voltage, Batteries 2 (2).
[72] C. Chen, R. Xiong, R. Yang, W. Shen, F. Sun, State-of-charge estimation of lithium-ion battery using an improved neural network model and extended Kalman filter, Journal of Cleaner Production 234 (2019) 1153–1164.
[73] F. Yang, W. Li, C. Li, Q. Miao, State-of-charge estimation of lithium-ion batteries based on gated recurrent neural network, Energy 175 (2019) 66–75.
[74] G. L. Plett, Battery Management System Volume II Equivalent-circuit Methods, artech hou Edition, 2016.
[75] Q. Zhu, M. Xu, W. Liu, M. Zheng, A state of charge estimation method for lithium-ion batteries based on fractional order adaptive extended kalman filter, Energy 187 (2019) 115880.

[76] F. Guo, G. Hu, S. Xiang, P. Zhou, R. Hong, N. Xiong, A multi-scale parameter adaptive method for state of charge and parameter estimation of lithium-ion batteries using dual Kalman filters, Energy 178 (2019) 79–88.